

# Stark localization near Aubry-André criticality

Ayan Sahoo,<sup>1</sup> Aitijhya Saha,<sup>1</sup> and Debraj Rakshit<sup>1</sup>

<sup>1</sup>Harish-Chandra Research Institute, A CI of Homi Bhabha National Institute, Chhatnag Road, Jhansi, Allahabad 211 019, India

(Dated: April 24, 2024)

In this work we investigate the Stark localization near the Aubry-André (AA) critical point. We study system-dependent parameters, such as localization length, inverse participation ratio (IPR), and energy gap between the ground and first excited state, for characterizing the localization-delocalization transition. We show that the scaling exponents possessed by these key descriptors of localization are quite different from that of a pure AA model or Stark model. Near the critical point of the AA model, inducing Stark field of strength  $h$ , the localization length  $\zeta$  scales as  $\zeta \propto h^{-\nu}$  with  $\nu \approx 0.29$  which is different than both the pure AA model ( $\nu = 1$ ) and Stark model ( $\nu \approx 0.33$ ). The IPR scales as  $\text{IPR} \propto h^s$  with  $s \approx 0.096$  which is again significantly different than both the pure AA model ( $s \approx 0.33$ ) and Stark model ( $s \approx 0.33$ ). The energy gap,  $\Delta$ , scales as  $E \propto h^{\nu z}$ , where  $z \approx 2.37$  which is however same as the pure AA model.

## I. INTRODUCTION

Randomness is an inherent property of nature whose influence on any physical system often defies our intuition and yields non-trivial effects. Consequently, disordered systems have long been a focal point of significant research endeavors [1–6]. Within the realm of quantum mechanics, the interplay of disorder with fundamental principles gives rise to a myriad of noteworthy phenomena, including the emergence of novel quantum phases, order-from-disorder phenomena [7–11], the enigmatic high- $T_c$  superconductivity [12], and the phenomenon of localization [13–18]. Among these phenomena, disorder-induced Anderson localization occupies a prominent position [19, 20]. This well-established concept elucidates how the presence of randomness can hinder the diffusion of waves within a system, showcasing its pivotal role in modern condensed matter physics. In Anderson model the disorder is truly random and uncorrelated. Whereas some disorders are not random, rather there is some correlation. Quasi-periodicity is the candidate that qualifies for this correlated disorder.

In the recent past and even nowadays quasiperiodic systems [21, 22] are widely studied as it captures very exotic features of various novel phases of matter and supports phase transition between those states [23–27]. Among these models, the Aubry-André (AA) [28, 50] model is of central interest of researchers for its distinct characteristics in the realm of phase transitions [29, 30]. One of the distinguishing features of the AA model is its self-dual symmetry, evident between the Hamiltonian formulations in momentum and position spaces. This symmetry manifests in an energy-independent localization-delocalization transition [31, 32] occurring at a finite modulation strength. This model has been extensively explored across various contexts, including the elucidation of the Hofstadter butterfly structure of the energy spectrum under controlled parameters [33], investigations into transport phenomena [34, 35], analysis of mobility edges [36–38], critical behavior, and exploration of topological phases [39–41], many-body localization [42–44], dynamical phase transition [45], in context of open quantum system [46–49], and for its applications in quantum technology [50]. The AA model has been realized using ultracold atoms in an incommensurate op-

tical lattice [51–53] and photonic lattices [54].

The AA model is a tight binding model with nearest neighbour tunnelling in the presence of sinusoidal quasi-periodic potential. When the strength of the potential becomes twice the tunneling parameter, in the thermodynamic limit, the system experiences a phase transition from a delocalized phase to a localized phase. On the other hand, in a tight binding model, if a gradient field is induced across the lattice making the on-site energies off-resonant, the tunnelling rate gets suppressed resulting in the localization of wavefunction in space in absence of disorder. In the thermodynamic limit, this localization, known as Stark localization [55], takes place at zero field limit. A substantial amount of research has been conducted for understanding Stark localization phenomena in context of single-particle [56–62] and many-body [63–67] systems, and for finding applications [68–72] by exploiting it.

All these are quantum phase transitions that manifest at zero temperature when the control parameter of a quantum system's Hamiltonian is finely tuned to a critical value, referred to as the quantum critical point (QCP). At this juncture, the system exhibits scaling and universality [73–79], meaning that the equilibrium properties of certain physical observables near the QCP can be succinctly described by a handful of critical exponents. Extracting these critical exponents necessitates an understanding of various physical quantities [80–82], such as the localization length, Inverse Participation Ratio (IPR), energy gap, and fidelity susceptibility etc. These quantities provide essential insights into the behavior of the system near the QCP and facilitate the characterization of its critical behavior. In this work, we consider a single particle tight-binding model with nearest-neighbour hopping. The system is prepared at the QCP of the AA model. Then a Stark potential is introduced for studying the scaling properties of localization length, IPR, and energy gap between the ground and the first excited state.

Following an introductory overview in Section I, Section II presents the model of our system. In Section III, defining the characteristic quantities relevant to the localization-delocalization transition, the behavior of the corresponding scaling exponents at the criticality of the AA model is studied via the cost function approach. In Section IV the same scaling exponents are computed in the vicinity of the critical point of the AA model. In Section V, we explore the evolu-

tion of the scaling exponent of IPR as we move away from the critical region of the AA model and additionally, we discuss how the corresponding structures of the wave function change. Then in Section VI, we introduce a hybrid scaling exponent that is related to the other scaling exponents of the pure AA and Stark model. Finally, a conclusion is given in Section VII.

## II. MODEL

The Hamiltonian of the Aubry-André model with a linear gradient field across the lattice, is

$$\hat{H} = -J \sum_i^L (\hat{c}_i^\dagger \hat{c}_{i+1} + \text{h.c.}) + h \sum_i^L i \hat{c}_i^\dagger \hat{c}_i + (2J + \delta) \sum_i^L \cos[2\pi(i\omega + \phi)] \hat{c}_i^\dagger \hat{c}_i \quad (1)$$

where,  $\hat{c}_i^\dagger$  ( $\hat{c}_i$ ) is the fermionic creation (annihilation) operator at the  $i^{\text{th}}$  site,  $(2J + \delta)$  determines the amplitude of the quasiperiodic modulation,  $\omega$  is an irrational number has a special form of  $\omega = F_n/F_{n+1}$  where  $F_n$  are the Fibonacci numbers and system size  $L$  has been chosen as  $L = F_{n+1}$ ,  $\phi$  is a random number resulting in some random phase of quasiperiodic potential, drawn from a uniform distribution in  $[0, 1)$ , and  $h$  quantifies the magnitude of the Stark field. The boundary condition used in this work is the open boundary condition (OBC). In the thermodynamic limit (i.e.,  $L \rightarrow \infty$ ) for the absence of the second term, i.e.,  $h = 0$ , one finds that all the eigenstates are localized for  $\delta > 0$  and all the eigenstates are delocalized for  $\delta < 0$ . On the other hand, without the last term i.e.,  $\delta = -2J$ , in the thermodynamic limit, the system is localized for  $h \rightarrow 0$ .

## III. SCALING ANALYSIS AT THE AA CRITICALITY

We start our study of the behaviour of the scaling exponents right at the AA criticality, i.e.,  $\delta = 0$ . In a finite system, at this point, the wavefunction of the particle is neither localized nor delocalized, rather there happens to be a continuous phase transition. To quantify the localized or delocalized nature of the wavefunction, we use the observable localization length,  $\zeta$ , defined as,

$$\zeta = \sqrt{\sum_i^L (i - i_c)^2 p_i}, \quad (2)$$

where  $i$  denotes the lattice site,  $p_i$  is the single-particle probability density at site  $i$  and  $i_c$  is the localization center having the expression  $i_c = \sum_{i=1}^L i p_i$ . Expanding the  $n^{\text{th}}$  normalised eigenstate of the system,  $|\psi^n\rangle$ , in terms of the single-particle computational basis,  $|i\rangle$ , such that  $|\psi^n\rangle = \sum_i c_n^{(i)} |i\rangle$ ,  $p_i$  is given by  $p_i = |\langle i|\psi^n\rangle|^2 = |c_n^{(i)}|^2$ . If  $g$  is the control param-

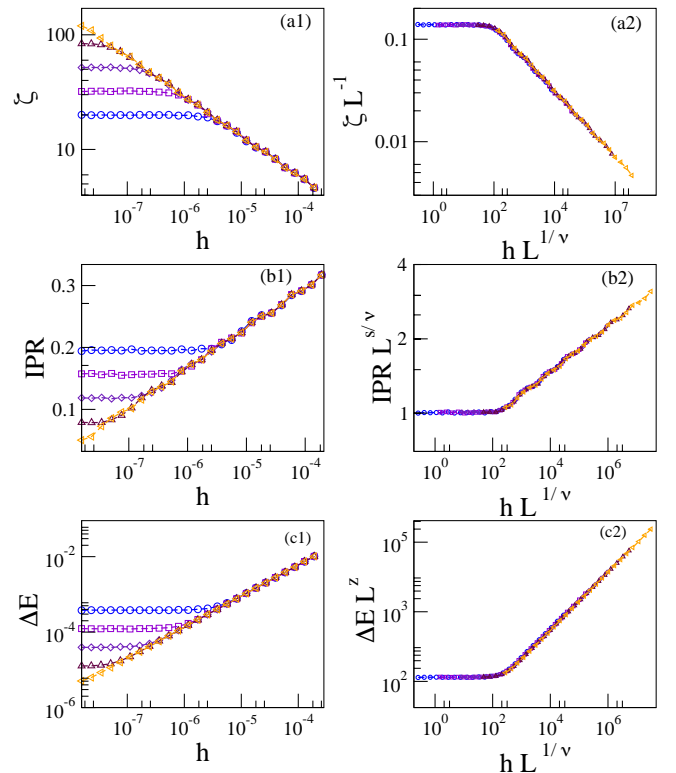


FIG. 1. **Scaling Analysis at  $\delta = 0$ :** (a1) presents localization length  $\zeta$  of the ground state against Stark field strength  $h$  for different system sizes,  $L = 144$  (blue circle),  $L = 233$  (violet square),  $L = 377$  (indigo diamond),  $L = 610$  (maroon triangle up) and  $L = 987$  (orange triangle left). (a2) shows a collapse plot for the localization length with the value of scaling exponent  $\nu = 0.29$ . (b1) displays the IPR versus  $h$  for various values of  $L$  which is aforementioned in (a1). (b2) demonstrates the collapse plot of IPR using the value of scaling exponent  $s = 0.096$  and  $\nu = 0.29$ . (c1) shows the energy gap  $\Delta E$  between the ground state and the first excited state as a function of  $h$  for different  $L$  values as mentioned previously. (c2) demonstrates the collapse plot of  $\Delta E$  using the scaling exponent  $z = 2.37$ . We have taken  $\phi$  average for 5000 random choices in the range  $[0, 1)$ .

eter in a certain localization-delocalization transition and  $g_c$  is the critical point then in the thermodynamic limit, near this criticality, the localization length scales as,

$$\zeta \propto |g - g_c|^{-\nu}, \quad (3)$$

where  $\nu$  is the scaling exponent. For the pure AA model,  $|g - g_c| = \delta$  and  $\nu = 1$ ; for the pure Stark model  $|g - g_c| = h$  and  $\nu \approx 0.33$ . Near criticality, the localization length scales with system size as,

$$\zeta \propto L^{-1}. \quad (4)$$

We study the dependence of the localization length  $\zeta$ , of the ground state, on the control parameter  $h$  for different system sizes  $L$ . For localization length, we adopt the following scaling ansatz,

$$\zeta/L = f_1(hL^{1/\nu}) \quad (5)$$

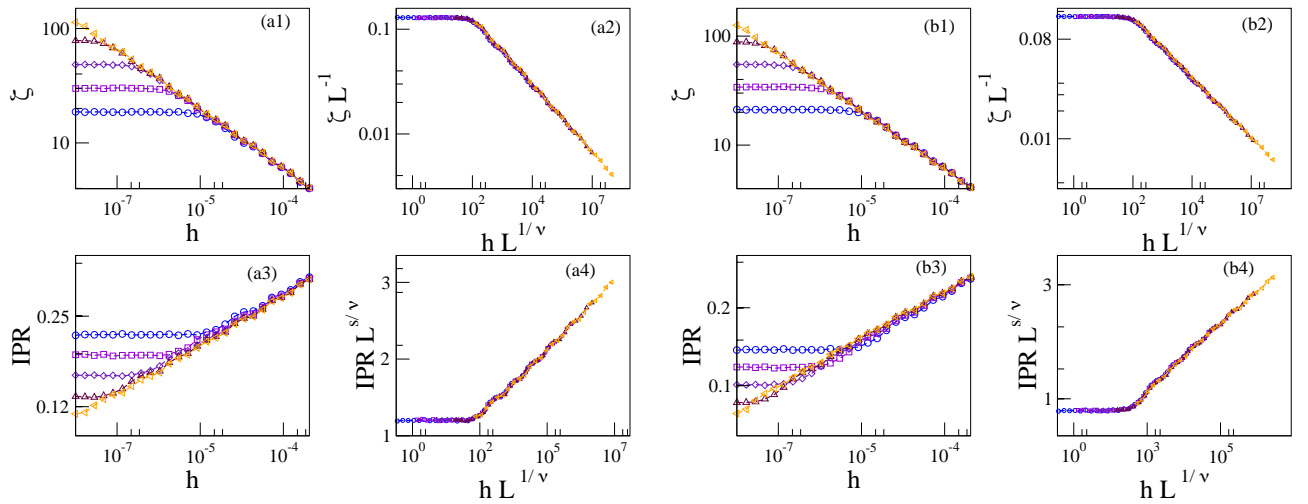


FIG. 2. **Scaling Analysis for  $\delta L^{1/\nu} = 1$ :** (a1) presents localization length  $\zeta$  against the Stark field of strength  $h$  for different system sizes,  $L = 144$  (blue circle),  $L = 233$  (violet square),  $L = 377$  (indigo diamond),  $L = 610$  (maroon triangle up),  $L = 987$  (orange triangle left). (a2) shows the corresponding collapse plot for a value of the scaling exponent  $\nu = 0.29$ . (a3) displays the IPR versus  $h$  for various values of  $L$  which is aforementioned in (a1). (a4) demonstrates the collapse plot of IPR using the scaling exponent value  $s = 0.096$ . **Scaling Analysis for  $\delta L^{1/\nu} = -1$ :** (b1) presents localization length  $\zeta$  against stark potential strength  $h$  for different system sizes,  $L$  with the same line-point scheme as before. (b2) shows the collapse plot for a value of scaling exponent  $\nu = 0.29$ . (b3) displays the IPR versus  $h$  for various values of  $L$  which is aforementioned in (a1). (b4) demonstrates the collapse plot of IPR using the scaling exponent value  $s = 0.096$ .

where  $f_1[\cdot]$  is an arbitrary function. This scaling ansatz is confirmed through the methodology of data collapse. The concept behind data collapse is as follows: We collect the data  $\zeta/L$  versus  $hL^{1/\nu}$  for various system sizes  $L$ , with a specific value of  $\nu$ , for which all the datasets collapse perfectly. Initially, by some trial and error, we manually find out a rough range of the scaling exponent for which the data collapse is quite well. Furthermore, for a better estimation of the scaling exponent we employ the cost function approach [83], where the cost function  $C_Q$  is defined as,

$$C_Q = \frac{\sum_{i=1}^{N_p-1} |Q_{i+1} - Q_i|}{\max\{Q_i\} - \min\{Q_i\}} - 1, \quad (6)$$

where  $\{Q_i\}$  is the dataset for different values of  $h$  and  $L$  and  $N_p$  is the total number of data points in the dataset. Sorting all  $N_p$  values of  $|Q_i|$  according to the increasing value of  $L \operatorname{sgn}[h - h_c][h - h_c]^\nu$ , the best scaling exponent can be found for the minimum value of cost function  $C_Q$ . Ideally, the perfect data collapse is found for  $C_Q = 0$ , i.e.,  $\sum_{i=1}^{N_p-1} |Q_{i+1} - Q_i| = \max\{Q_i\} - \min\{Q_i\}$ .

In Fig. 1(a1), we depicted  $\zeta$  against  $h$  for various values of  $L$ . This figure illustrates that for finite-sized systems, an initial flat region exists wherein the corresponding wave function exhibits an extended nature, indicating that the ground state of the Hamiltonian for  $\delta = 0$  is equally probable across this phase. Beyond a certain threshold of  $h$ , the localization length exhibits weak dependence on the system size, leading to the localization of the wavefunction. To derive the scaling exponent  $\nu$  from Eq. (3) with  $|g - g_c| = h$ , we demonstrate a collapse plot in Fig. 1(a2) utilizing the function specified previously in Eq. (5). The best collapse is obtained for  $\nu = 0.29(1)$ . The cost function approach further confirms this

optimal value of the scaling exponent  $\nu$ .

The next observable that can capture the delocalization-localization transition is the IPR, defined as,

$$\text{IPR} = \sum_{i=1}^L p_i^2. \quad (7)$$

Near criticality, in the thermodynamic limit, the IPR scales as,

$$\text{IPR} \propto |g - g_c|^s, \quad (8)$$

where  $s$  is another scaling exponent. For the pure AA model,  $|g - g_c| = \delta$  and  $s \approx 0.33$ ; for the pure Stark model  $|g - g_c| = h$  and  $s \approx 0.33$ . On the other hand, near criticality, IPR scales with system size  $L$  as,

$$\text{IPR} \propto L^{-s/\nu}. \quad (9)$$

So for IPR, the scaling ansatz we use is,

$$\text{IPR} = L^{-s/\nu} f_2(hL^{1/\nu}), \quad (10)$$

where  $f_2[\cdot]$  is another arbitrary function.

The variation in the value of IPR with the increase in  $h$  for different system sizes  $L$  is depicted in Fig. 1(b1). In this figure, upto a certain region of  $h$ , the IPR values appear flat, indicating the presence of a delocalized phase. Beyond this region, the IPR becomes independent of the system size, characterizing the localized phase. We employ the cost function approach which suggests  $s = 0.096(1)$ . Fig. 1(b2) presents the best collapse plot of the IPR using  $s = 0.096$ . Noticeably, in this case,  $s/\nu \approx 0.33$  which is the same as the pure AA model demonstrating the fact that at the criticality the scaling

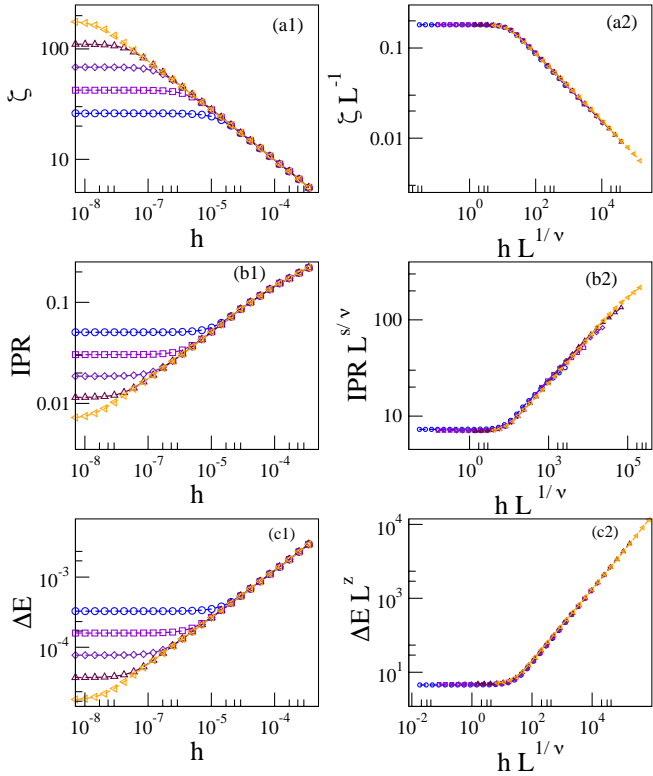


FIG. 3. **Scaling Analysis for  $\delta = -0.1$ :** (a1) presents localization length  $\zeta$  against stark potential strength  $h$  for different system size  $L$ , with the same line-point scheme. (a2) shows the collapse plot for a value of the scaling exponent  $\nu = 0.33$ . (b1) displays the IPR versus  $h$  for various values of  $L$ . (b2) demonstrates the collapse plot of IPR with  $s = 0.33$ . (c1) depicts the variation of  $\Delta E$  as a function of  $h$  for different  $L$ 's. (c2) demonstrates the collapse plot of  $\Delta E$  using the scaling exponent  $z = 2$  as before.

of IPR with the system size is the same for both of these two models. Finally, to elucidate the localization transition, we examine the energy gap between the ground state and the first excited energy, denoted as  $\Delta E$ . In the thermodynamic limit, the energy gap scales with the control parameter as,

$$\Delta E \propto |g - g_c|^{\nu z}. \quad (11)$$

For the pure AA model  $z = 2.37$  and for the pure Stark model  $z = 2$ . To perform the finite size scaling for  $\Delta E$ , we use the scaling ansatz:

$$\Delta E = L^{-z} f_3(hL^{1/\nu}), \quad (12)$$

where  $f_3[\cdot]$  is another arbitrary function.

Fig. 1(c1) shows, the energy gap  $\Delta E$  against the Stark field strength  $h$  for different system sizes. In this case, also there is an initial flat region showing a very narrow energy gap in the delocalized phase. Beyond a certain strength of Stark field  $h$ ,  $\Delta E$  becomes independent of the system size and the energy gap gets increased with an increase in the field strength. The scaling exponent  $z$  is determined through data collapse yielding a critical exponent of  $z = 2.37(1)$ . It is also the same as the pure AA model. The collapse plot corresponding to  $\Delta E$  is presented in Fig. 1(c2).

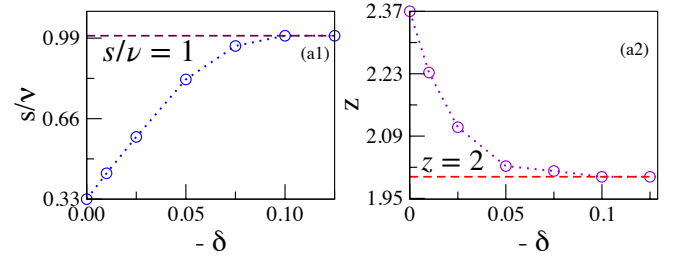


FIG. 4. (a1) presents  $s/\nu$  for different values of  $\delta$ . For  $\delta = 0$  the  $s/\nu$  value is 0.33 which is the same as that of the pure AA model and this value continuously increases to 1, which is the same as the pure Stark model, as one moves away from the AA criticality with negative  $\delta$  values. (a2) presents the plot of  $z$  for different values of  $\delta$ . In this case also, there is a continuous change in the value of  $s/\nu$  from 2.37, which is the same as the pure AA model, to 2, which is for the pure Stark model, as one moves away from the criticality.

#### IV. SCALING PROPERTIES NEAR AA CRITICALITY

In the previous section, we have done the scaling analysis at the AA criticality, i.e.,  $\delta = 0$ . Now we turn our attention to the near criticality region of the AA model. Now as  $\delta \neq 0$  one can expect that the previous scaling ansatz will not work properly and some modifications are needed.

We start with the scaling of localization length. In the presence of both  $\delta$  and  $h$ , we use the following ansatz for the scaling of localization length,

$$\zeta/L = f_4(\delta L^{1/\nu_\delta}, hL^{1/\nu}), \quad (13)$$

where  $\nu_\delta$  is the scaling exponent for localization length in the case of a pure AA model. The novelty of this ansatz is that when  $\delta = 0$ , it coincides with the ansatz given in Eq. (5), and for  $h = 0$ , it becomes the scaling ansatz for pure AA model, i.e.,  $\zeta \propto \delta^{-\nu_\delta}$ , in the thermodynamic limit.

In the same spirit, we define the scaling ansatz for IPR as,

$$\text{IPR} = L^{-s_\delta/\nu_\delta} f_5(\delta L^{1/\nu_\delta}, hL^{1/\nu}) \quad (14)$$

where  $s_\delta$  is the scaling exponent of IPR in the pure AA model ( $h = 0$ ), i.e.,  $\text{IPR} \propto \delta^{s_\delta}$ , in the thermodynamic limit. When  $\delta = 0$ , this scaling ansatz takes the similar form used in the previous section for the collapse as we have found that the  $s/\nu$  value is the same for both the pure AA model and our model under consideration. Similarly, for  $\Delta E$  it will take the form,

$$\Delta E = L^{-z_\delta} f_6(\delta L^{1/\nu_\delta}, hL^{1/\nu}), \quad (15)$$

where  $z_\delta$  appears in the scaling exponent of  $\Delta E$  in the pure AA model, i.e.,  $\Delta E \propto \delta^{\nu_\delta z_\delta}$ , in the thermodynamic limit, again this works due to the same value of  $z$  in both models. To examine the validation of the above scaling ansatz, we now turn our attention to delve into scaling properties of  $\zeta$ , IPR, and  $\Delta E$  near criticality for  $\delta L^{1/\nu} = 1$  and  $\delta L^{1/\nu} = -1$ . Upon taking  $\delta$  in this fashion for different  $L$ , we expect that our previous critical exponents would work as we are still in the vicinity of the AA critical point. In Fig. 2 both these cases

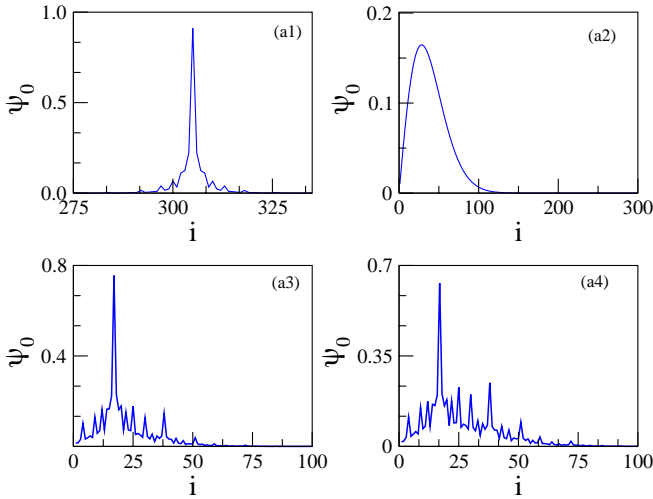


FIG. 5. **Ground State Wavefunction**  $\psi_0$ : **(a1)** describes the ground state wavefunction for the pure AA model, where  $h = 0$  and  $\delta = 0.4J$ . **(a2)** presents the ground state wavefunction for the pure Stark model, where  $\delta = -2J$  and  $h = 10^{-4}$ . **(a3)** presents the ground state wavefunction for  $\delta = 0$  with  $h = 10^{-4}$  and **(a4)** presents the wave function for  $\delta = -0.1$  and  $h = 10^{-4}$ . All plots are done for system size 610 and for the AA potential, the phase,  $\phi = 0$ .

are shown and we have numerically found that the collapse still happens for the same set of scaling exponents as found in the case of  $\delta = 0$ .

## V. SCALING ANALYSIS AT FAR FROM THE AUBRY-ANDRÉ CRITICALITY

Now we focus on the scaling analysis at comparatively far away from the AA criticality. Far from the AA criticality, the wavefunction is supposed to be delocalized as the effect of AA potential is faint at that region. In order to validate this understanding we perform a scaling analysis for a fixed value of  $\delta < 0$ , specifically  $\delta = -0.1$ , as illustrated in Fig. 3.

In Fig. 3(a1), the localization length ( $\zeta$ ) is plotted against  $h$ , while in Fig. 3(a2), we depict  $\zeta/L$  against  $hL^{1/\nu}$ , with a specific value of  $\nu = 0.33$ . Remarkably, all datasets collapse onto a single curve for this value of  $\nu$ . This observation suggests that in the as we move away from the AA criticality the scaling nature replicates the scaling of Stark localization. The IPR for  $\delta = -0.1$  across various system sizes is shown in Fig. 3(b1). Scaling analysis for IPR gives the value,  $s = 0.33$ , which is confirmed by data collapse shown in Fig. 3(b2) and also by the cost-function approach. This scaling exponent is identical to that of the pure Stark model. In Fig. 3(c1), we plot the dependence of  $\Delta E$  on  $h$ . The nature of the dependence is found to be the same as before. The collapse plot corresponding to  $\Delta E$  is depicted in Fig. 3(c2), yielding a critical exponent of  $z = 2.00(2)$  which is again the same critical exponent value for that of the pure Stark model.

Thus, as we move away from the AA criticality the system does not experience much effect due to the AA potential. Likewise, the delocalization-localization transition is solely

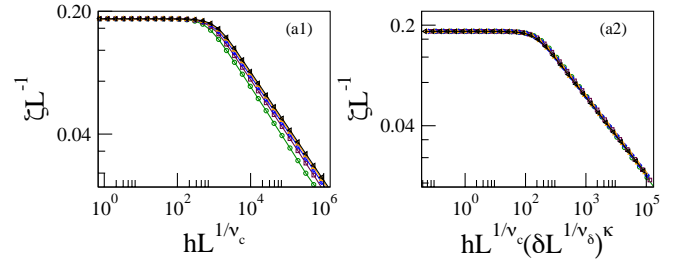


FIG. 6. In **(a1)**, we have plotted the curves of  $\zeta L^{-1}$  against  $hL^{1/\nu_c}$  for fixed system size,  $L = 377$ , having various  $\delta$  values:  $\delta = -0.1$  (green circle),  $\delta = -0.2$  (maroon square),  $\delta = -0.3$  (blue diamond),  $\delta = -0.4$  (orange triangle up), and  $\delta = -0.5$  (black triangle left). Here  $\nu_c = 0.29$ , the value of scaling exponent for localization length at the AA criticality, i.e.,  $\delta = 0$ . **(a2)** shows the collapse plot of  $\zeta L^{-1}$  versus  $hL^{1/\nu_c}(\delta L^{1/\nu_\delta})^\kappa$ . Here also, we have taken  $\phi$  average for 5000 choices.

controlled by the Stark field. Therefore we study the behaviour of the scaling exponents as we slowly move away from the criticality. Fig. 4 nicely depicts this variation. The variation of  $s/\nu$  and  $z$  are shown in Fig. 4(a1) and Fig. 4(a2) respectively. To be specific, here, we only focus on the negative values of  $\delta$ , as we have found that a slight departure from the critical point in the positive  $\delta$  values results in a very weird kind of variation in the characteristic observables and as a consequence of that, the scaling analysis fails there. This happens due to the competition between the two kinds of localization. From Fig. 4 it is easily noticeable that in the negative  $\delta$  region, there is a continuous change in the values of the scaling exponents. As we move away from the AA criticality, the values of  $s/\nu$  and  $z$  slowly change from that of the pure AA model to the pure Stark model.

Moreover, in order to understand the competing nature of two distinct types of localization inducing potentials closely, it is interesting to directly look into the structures of the ground state wavefunctions for various cases. We present some exemplary cases in Fig. 5 for various scenarios relevant to our study of the scaling nature of the system near the criticality.

## VI. HYBRID SCALING EXPONENT

Next, we focus on a case, where the system size,  $L$ , is kept fixed and different  $\delta$  values are considered with  $\delta < 0$ . For this case, we use the following scaling ansatz,

$$\zeta/L = f_\tau(hL^{1/\nu_c}(\delta L^{1/\nu_\delta})^\kappa), \quad (16)$$

where  $\nu_c$  is the scaling exponent for the localization length of the ground state in our model, at the AA criticality, i.e.,  $\delta = 0$ . Here we numerically find out the new scaling exponent  $\kappa$ . Near AA criticality, this  $\kappa$  should have the following form,

$$\kappa = \nu_\delta(1/\nu_s - 1/\nu_c), \quad (17)$$

where  $\nu_\delta$  and  $\nu_s$  are the critical exponents for the localization length in the case of pure AA and Stark model.

In Fig. 6(a1), we show the variation of  $\zeta/L$  against  $hL^{1/\nu_c}$  for different values of  $\delta$ . Fig. 6(a2) shows that the collapse plot of  $\zeta L^{-1}$  as a function of the hybrid quantity  $hL^{1/\nu_c}(\delta L^{1/\nu_\delta})^\kappa$ . From the cost function approach, we have found the scaling exponent  $\kappa = -0.418(2)$  which matches with the value obtained via Eq. 17.

## VII. CONCLUSION

In this work we have explored the Stark localization in the presence of a quasi-periodic potential, namely the AA potential. This exploration is based on the scaling analysis of finite-size systems. First, we have studied the effect of increasing Stark field at the AA criticality. We have found that the scaling exponents  $\nu$  and  $s$  are quite different than both the pure AA model and the pure Stark model. However, the  $s/\nu$  value is found to be the same as that of the pure AA model.

Also, the scaling exponent  $z$  is identical to that of the pure AA model. It indicates although the Stark field drives the transition, the transition is mostly AA type. Next, we have studied the same near the AA criticality. As in that case, we have used  $\delta \neq 0$ , we cannot employ the scaling ansatz for one control parameter-based phase transition. We have developed some scaling ansatz that is capable of extracting the relevant scaling exponents quite efficiently. Then, we take a fixed system size and vary the distance from the AA criticality. For this, a hybrid scaling ansatz is used and it successfully describes the scaling nature. Finally, we have looked into the variation of  $s/\nu$  and  $z$  with negative values of  $\delta$  which have revealed the fact that near the AA criticality, these exponents coincide with that of the pure AA model, and as we move away from the AA criticality we enter into the region where the localization is solely driven by Stark field with almost no trace of the presence of AA potential.

- 
- [1] K. Binder and A. P. Young, Spin glasses: Experimental facts, theoretical concepts, and open questions, *Rev. Mod. Phys.* **58**, 801 (1986).
  - [2] D. Belitz, T. R. Kirkpatrick, and T. Vojta, How generic scale invariance influences quantum and classical phase transitions, *Rev. Mod. Phys.* **77**, 579 (2005).
  - [3] A. Das and B. K. Chakrabarti, Colloquium: Quantum annealing and analog quantum computation, *Rev. Mod. Phys.* **80**, 1061 (2008).
  - [4] H. Alloul, J. Bobroff, M. Gabay, and P. J. Hirschfeld, Defects in correlated metals and superconductors, *Rev. Mod. Phys.* **81**, 45 (2009).
  - [5] T. K. Konar, S. Ghosh, A. K. Pal, and A. Sen(De), Designing robust quantum refrigerators in disordered spin models, *Phys. Rev. A* **105**, 022214 (2022).
  - [6] P. Ghosh, K. Sen, U. Sen, Response to glassy disorder in coin on spread of quantum walker, arXiv:2111.09827
  - [7] M. Aizenman and J. Wehr, Rounding of first-order phase transitions in systems with quenched disorder, *Phys. Rev. Lett.* **62**, 2503 (1989).
  - [8] J. Wehr, A. Niederberger, L. Sanchez-Palencia, and M. Lewenstein, Disorder versus the Mermin-Wagner-Hohenberg effect: From classical spin systems to ultracold atomic gases, *Phys. Rev. B* **74**, 224448 (2006).
  - [9] A. Bera, D. Rakshit, M. Lewenstein, A. Sen(De), U. Sen, and J. Wehr, Classical spin models with broken symmetry: Random-field-induced order and persistence of spontaneous magnetization in the presence of a random field, *Phys. Rev. B* **90**, 174408 (2014).
  - [10] A. Bera, D. Rakshit, M. Lewenstein, A. Sen(De), U. Sen, and J. Wehr, Disorder-induced enhancement and critical scaling of spontaneous magnetization in random-field quantum spin systems, *Phys. Rev. B* **94**, 014421 (2016).
  - [11] A. Bera, D. Rakshit, A. Sen(De), and U. Sen, Spontaneous magnetization of quantum XY spin model in joint presence of quenched and annealed disorder, *Phys. Rev. B* **95**, 224441 (2017).
  - [12] A. Auerbach, *Interacting electrons and quantum magnetism* (Springer, New York, 1994).
  - [13] P. W. Anderson, Absence of diffusion in certain random lattices, *Phys. Rev.* **109**, 1492 (1958).
  - [14] E. Abrahams, P. W. Anderson, D. C. Licciardello, and T. V. Ramakrishnan, Scaling theory of localization: Absence of quantum diffusion in two dimensions, *Phys. Rev. Lett.* **42**, 673 (1979).
  - [15] F. Evers and A. D. Mirlin, Anderson transitions, *Rev. Mod. Phys.* **80**, 1355 (2008).
  - [16] R. Nandkishore and D. A. Huse, Many-body localization and thermalization in quantum statistical mechanics, *Annu. Rev. Condens. Matter Phys.* **6**, 15 (2015).
  - [17] D. A. Abanin, E. Altman, I. Bloch, and M. Serbyn, Colloquium: many-body localization, thermalization, and entanglement, *Rev. Mod. Phys.* **91**, 021001 (2019)
  - [18] A. Saha, D. Rakshit, Localization with non-Hermitian off-diagonal disorder, arXiv:2310.13744.
  - [19] A. Yamilov, S. E. Skipetrov, T. W. Hughes, M. Minkov, Z. Yu, H. Cao, Anderson localization of electromagnetic waves in three dimensions, *Nature physics* **19**, 1308-1313 (2023).
  - [20] A. Lagendijk, B. van Tiggelen, and D. S. Wiersma, Fifty years of Anderson Localization, *Physics Today* **62**, 24 (2009).
  - [21] A. Sinha, M. M. Rams, and J. Dziarmaga, Kibble-Zurek mechanism with a single particle: Dynamics of the localization-delocalization transition in the Aubry-André model, *Phys. Rev. B* **99**, 094203 (2019).
  - [22] B. -B. Wei, Fidelity susceptibility in one-dimensional disordered lattice models, *Phys. Rev. A* **99**, 042117 (2019).
  - [23] D. Chowdhury, *Spin Glasses and other Frustrated Systems* (Wiley, New York, 1086).
  - [24] M. Mezard, G. Parisi, and M.A. Virasoro, *Spin Glass Theory and Beyond* (World Scientific, Singapore, 1987).
  - [25] S. Sachdev, *Quantum Phase Transitions* (Cambridge University Press, Cambridge, 1999).
  - [26] Z. Yao, K. P. C. da Costa, M. Kiselev, and N. Prokof'ev, Critical exponents of the superfluid-Bose-glass transition in three dimensions, *Phys. Rev. Lett.* **112**, 225301 (2014).
  - [27] J. P. Á. Zúñiga and N. Laflorencie, Bose-glass transition and spin-wave localization for 2D bosons in a random potential, *Phys. Rev. Lett.* **111**, 160403 (2013).

- [28] S. Aubry and G. André, Anderson localization for one-dimensional difference Schrödinger operator with quasiperiodic potential, *Ann. Isr. Phys. Soc.* **3**, 18 (1980).
- [29] P. Zanardi, P. Giorda, and M. Cozzini, Information-theoretic differential geometry of quantum phase transitions, *Phys. Rev. Lett.* **99**, 100603 (2007).
- [30] S. Mondal, G. Biswas, A. Ghoshal, A. Biswas, U. Sen, Estimating phase transition of perturbed  $J_1 - J_2$  Heisenberg quantum chain in mixtures of ground and first excited states, *New J. Phys.* **25**, 123020 (2023).
- [31] V. P. Michal, B. L. Altshuler, and G. V. Shlyapnikov, Delocalization of weakly interacting bosons in a 1D quasiperiodic potential, *Phys. Rev. Lett.* **113**, 045304 (2014).
- [32] S. Iyer, V. Oganesyan, G. Refael, and D. A. Huse, Many-body localization in a quasiperiodic system, *Phys. Rev. B* **87**, 134202 (2013).
- [33] D. R. Hofstadter, Energy levels and wave functions of Bloch electrons in rational and irrational magnetic fields, *Phys. Rev. B* **14**, 2239 (1976).
- [34] A. Purkayastha, S. Sanyal, A. Dhar, and M. Kulkarni, Anomalous transport in the Aubry-André-Harper model in isolated and open systems, *Phys. Rev. B* **97**, 174206 (2018).
- [35] J. Sutradhar, S. Mukerjee, R. Pandit, and S. Banerjee, Transport, multifractality, and the breakdown of single-parameter scaling at the localization transition in quasiperiodic systems, *Phys. Rev. B* **99**, 224204 (2019).
- [36] S. Saha, S. K. Maiti, and S. Karmakar, Multiple mobility edges in a 1D Aubry chain with Hubbard interaction in presence of electric field: Controlled electron transport, *Physica E* **83**, 358 (2016).
- [37] S. Ganeshan, J. H. Pixley, and S. Das Sarma, Nearest neighbor tight binding models with an exact mobility edge in one dimension, *Phys. Rev. Lett.* **114**, 146601 (2015).
- [38] X. Li, S. Ganeshan, J. H. Pixley, and S. Das Sarma, Many-Body localization and quantum nonergodicity in a model with a single-particle mobility edge, *Phys. Rev. Lett.* **115**, 186601 (2015).
- [39] W. DeGottardi, D. Sen, and S. Vishveshwara, Majorana fermions in superconducting 1D systems having periodic, quasiperiodic, and disordered potentials, *Phys. Rev. Lett.* **110**, 146404 (2013).
- [40] X. Cai, L.-J. Lang, S. Chen, and Y. Wang, Topological superconductor to Anderson localization transition in one-dimensional incommensurate lattices, *Phys. Rev. Lett.* **110**, 176403 (2013).
- [41] J. Fraxanet, U. Bhattacharya, T. Grass, D. Rakshit, M. Lewenstein and A. Dauphin, Topological properties of the long-range Kitaev chain with Aubry-André-Harper modulation, *Phys. Rev. Res.* **3**, 013148 (2021).
- [42] S.-J. Gu and W. C. Yu, Spectral function and fidelity susceptibility in quantum critical phenomena, *Europhys. Lett.* **108**, 20002 (2014).
- [43] J. Zhang, X. Peng, N. Rajendran, and D. Suter, Detection of quantum critical points by a probe qubit, *Phys. Rev. Lett.* **100**, 100501 (2008).
- [44] J. Zhang, F. M. Cucchiatti, C. M. Chandrashekar, M. Laforest, C. A. Ryan, M. Ditty, A. Hubbard, J. K. Gamble, and R. Laflamme, Direct observation of quantum criticality in Ising spin chains, *Phys. Rev. A* **79**, 012305 (2009).
- [45] R. Modak and D. Rakshit, Many-body dynamical phase transition in quasi-periodic potential, *Phys. Rev. B* **103**, 224310 (2021).
- [46] H. J. Carmichael, *Phys. Rev. Lett.* Quantum trajectory theory for cascaded open systems, **70**, 2273 (1993).
- [47] H. Xu, D. Mason, L. Jiang, and J. Harris, Topological energy transfer in an optomechanical system with exceptional points, *Nature* **537**, **80** (2016).
- [48] K. Kawabata, Y. Ashida, and M. Ueda, Information retrieval and criticality in parity-time-symmetric systems, *Phys. Rev. Lett.* **119**, 190401 (2017).
- [49] J. Y. Lee, J. Ahn, H. Zhou, and A. Vishwanath, Topological correspondence between Hermitian and non-Hermitian systems: Anomalous dynamics, *Phys. Rev. Lett.* **123**, 206404 (2019).
- [50] A. Sahoo, U. Mishra, and D. Rakshit, Localization-driven quantum sensing, *Phys. Rev. A* **109**, L030601 (2024).
- [51] K. G. Makris, R. El-Ganainy, D. N. Christodoulides, and Z. H. Musslimani, Beam dynamics in PT symmetric optical lattices, *Phys. Rev. Lett.* **100**, 103904 (2008).
- [52] S. Klaiman, U. Günther, and N. Moiseyev, Visualization of branch points in PT-symmetric waveguides, *Phys. Rev. Lett.* **101**, 080402 (2008).
- [53] C. E. Ruter, K. G. Makris, R. El-Ganainy, D. N. Christodoulides, M. Segev, and D. Kip, Observation of parity-time symmetry in optics, *Nat. Phys.* **6**, 192 (2010).
- [54] G. Roati, C. D'Errico, L. Fallani, M. Fattori, C. Fort, M. Zaccanti, G. Modugno, M. Modugno, and M. Inguscio, Anderson localization of a non-interacting Bose-Einstein condensate, *Nature* **453**, 895 (2008).
- [55] M. Schulz, C. A. Hooley, R. Moessner, and F. Pollmann, Stark many-body localization, *Phys. Rev. Lett.* **122**, 040606 (2019).
- [56] G. H. Wannier, Wave functions and effective Hamiltonian for Bloch electrons in an electric field, *Phys. Rev.* **117**, 432 (1960).
- [57] H. Fukuyama, R. A. Bari, and H. C. Fogedby, Tightly bound electrons in a uniform electric field, *Phys. Rev. B* **8**, 5579 (1973).
- [58] M. Holthaus, G. Ristow, and D. Hone, Random lattices in combined a.c. and d.c. electric fields: Anderson vs. Wannier-Stark localization, *Europhys. Lett.* **32**, 241 (1995).
- [59] A. R. Kolovsky and H. J. Korsch, Bloch oscillations of cold atoms in two-dimensional optical lattices, *Phys. Rev. A* **67**, 063601 (2003).
- [60] A. R. Kolovsky, Interplay between Anderson and Stark Localization in 2D Lattices, *Phys. Rev. Lett.* **101**, 190602 (2008).
- [61] A.R. Kolovsky and E. N. Bulgakov, Wannier-Stark states and Bloch oscillations in the honeycomb lattice, *Phys. Rev. A* **87**, 033602 (2013).
- [62] E. van Nieuwenburg, Y. Baum, and G. Refael, From Bloch oscillations to many-body localization in clean interacting systems, *Proc. Natl. Acad. Sci. U.S.A.* **116**, 9269 (2019).
- [63] X. P. Jiang, R. Qi, S. Yang, Y. Hu, G. Yang, Stark many-body localization with long-range interactions, *arXiv:2307.12376* (2023).
- [64] L. Zhang, Y. Ke, W. Liu, and C. Lee, Mobility edge of Stark many-body localization, *Phys. Rev. A* **103**, 023323 (2021).
- [65] R. Yao, T. Chanda, and J. Zakrzewski, Many-body localization in tilted and harmonic potentials, *Phys. Rev. B* **104**, 014201 (2021).
- [66] X. Wei, X. Gao, and W. Zhu, Static and dynamical Stark many-body localization transition in a linear potential, *Phys. Rev. B* **106**, 134207 (2022).
- [67] E. V. H. Doggen, I. V. Gornyi, and D. G. Polyakov, Stark many-body localization: Evidence for hilbert-space shattering, *Phys. Rev. B* **103**, L100202 (2021).
- [68] W. Morong, F. Liu, P. Becker, K. Collins, L. Feng, A. Kyprianiadis, G. Pagano, T. You, A. Gorshkov, and C. Monroe, Observation of Stark many-body localization without disorder, *Nature* **599**, 393 (2021).

- [69] P. M. Preiss, R. Ma, M. E. Tai, A. Lukin, M. Rispoli, P. Zupanic, Y. Lahini, R. Islam, and M. Greiner, Strongly correlated quantum walks in optical lattices, *Science* **347**, 1229 (2015).
- [70] A. H. Karamlou, J. Braumüller, Y. Yanay, A. Di Paolo, P. M. Harrington, B. Kannan, D. Kim, M. Kjaergaard, A. Melville, S. Muschinske et al., Quantum transport and localization in 1d and 2d tight-binding lattices, *npj Quantum Inf.* **8**, 35 (2022).
- [71] X. He, R. Yousefjani, and A. Bayat, Stark localization as a resource for weak-field sensing with super-Heisenberg precision, *Phys. Rev. Lett.* **131**, 010801 (2023).
- [72] T. Kohlert, S. Scherg, P. Sala, F. Pollmann, B. H. Madhusudhana, I. Bloch, M. Aidelsburger, Experimental realization of fragmented models in tilted Fermi-Hubbard chains, arXiv:2106.15586 (2021).
- [73] S. Hikami, Anderson localization in a nonlinear- $\sigma$ -model representation, *Phys. Rev. B* **24**, 2671 (1981).
- [74] A. Altland and M. R. Zirnbauer, Nonstandard symmetry classes in mesoscopic normal-superconducting hybrid structures, *Phys. Rev. B* **55**, 1142 (1997).
- [75] T. Wang, T. Ohtsuki, and R. Shindou, Universality classes of the Anderson transition in the three-dimensional symmetry classes AIII, BDI, C, D, and CI, *Phys. Rev. B* **104**, 014206 (2021).
- [76] X. Luo, T. Ohtsuki, and R. Shindou, Universality classes of the Anderson transitions driven by non-Hermitian disorder, *Phys. Rev. Lett.* **126**, 090402 (2021).
- [77] X. Luo, Z. Xiao, K. Kawabata, T. Ohtsuki, and R. Shindou, Unifying the Anderson transitions in Hermitian and non-Hermitian systems, *Phys. Rev. Res.* **4**, L022035 (2022).
- [78] X. Luo and T. Ohtsuki, Universality classes of the Anderson transitions driven by quasiperiodic potential in the three-dimensional Wigner-Dyson symmetry classes, *Phys. Rev. B* **106**, 104205 (2022).
- [79] X. Bu, L. -J. Zhai and S. Yin, Quantum criticality in the disordered Aubry-André model, *Phys. Rev. B* **106**, 214208 (2022).
- [80] U. Mishra, D. Rakshit, R. Prabhu, A. Sen De, U. Sen, Constructive interference between disordered couplings enhances multiparty entanglement in quantum Heisenberg spin glass models, *New J. Phys.* **18**, 083044 (2016).
- [81] D. Sadhukhan, S. S. Roy, D. Rakshit, A. Sen(De), and U. Sen, Beating no-go theorems by engineering defects in quantum spin models, *New J. Phys.* **17**, 043013 (2015).
- [82] D. Sadhukhan, S. S. Roy, D. Rakshit, R. Prabhu, A. Sen(De), and U. Sen, Quantum discord length is enhanced while entanglement length is not by introducing disorder in a spin chain, *Phys. Rev. E* **93**, 012131 (2016).
- [83] J. Suntajs, J. Bonca, T. Prosen, and L. Vidmar, Ergodicity breaking transition in finite disordered spin chains, *Phys. Rev. B* **102**, 064207 (2020).